PHYSICAL REVIEW B **77**, 064418 (2008)

Spin-glass transition in a La-doped Sr_2MnWO_6 double perovskite

A. K. Azad,[1] J. M. Wikberg,[2] S.-G. Eriksson,[3] A. Khan,[4] P. Svedlindh,[2] and J. T. S. Irvine[1]
[1]*School of Chemistry, University of St-Andrews, Fife KY16 9ST Scotland, United Kingdom*
[2]*Department of Engineering Sciences, Uppsala University, P.O. Box 534, SE-751 21 Uppsala, Sweden*
[3]*Department of Environmental Inorganic Chemistry, Chalmers University of Technology, SE-412 96 Göteborg, Sweden*
[4]*Department of Chemistry, University of Balochistan, Quetta 87300, Pakistan*

(Received 28 June 2007; revised manuscript received 2 November 2007; published 14 February 2008)

Polycrystalline $Sr_{2-x}La_xMnWO_6$ (x=0.25 and 0.5) materials have been prepared by a traditional solid state sintering method and studied by neutron powder diffraction (NPD) and magnetization measurements. Rietveld analysis of the temperature dependent NPD data shows that the compounds crystallize in monoclinic symmetry (space group $P2_1/n$). The unit cell volume decreases with increasing La^{3+} concentration at the A site. The crystal structure contains alternating MnO_6 and WO_6 octahedra, considerably tilted due to the relative small size of the cations that occupy the A sublattice of the perovskite. ac and dc magnetization measurements show a destruction of the low temperature antiferromagnetic phase by electron doping through substitution of Sr^{2+} for La^{3+}. The electron doping creates a mixed tungsten valence (W^{6+}/W^{5+}) resulting in a low temperature spin-glass state.

DOI: 10.1103/PhysRevB.77.064418 PACS number(s): 75.50.Lk, 61.05.fm

INTRODUCTION

Carrier doping in perovskites has been a very successful tool to disclose some of the most exciting new phenomena in materials research in the last few years. Manganese perovskites and high-T_C superconducting cuprates are among the most well-known examples. Recently, double-perovskite oxides of the type Sr_2FeMoO_6, half-metallic ferromagnets,[1–3] have received a great deal of attention because they display a substantial magnetoresistance and their Curie temperature is well above that observed for mixed-valence manganites. The modification of structural properties of B site ordered double-perovskite oxides, caused by a change of A-site and/or B-site cations, is also of great interest.[4,5] Depending on their valences and relative radii, the B site is often occupied by transition metals and can accommodate two different metal ions. The structure and physical properties of this type of double perovskite (general formula, $A_2B'B''O_6$) depend considerably on the valence of the B' and B'' cations. They can adopt a rich variety of crystallographic phases: e.g., cubic, tetragonal, and monoclinic. Moreover, both the magnetic properties and the structural distortion of the double perovskites strongly depend on the A-site cation. To give one example, depending on type of A-site cation, the system A_2MnWO_6 (Ba, Sr, Ca) shows cubic through tetragonal to monoclinic lattice symmetry[6–8] and the antiferromagnetic transition temperature increases from 9 to 16 K from Ba to Ca. Hence, these structural distortions are of interest not only from a crystallographer's point of view but also because they can have important effects on the physical properties of perovskite compounds, particularly on electrical and magnetic properties. In our earlier studies on A_2MnWO_6 (Ba, Sr, Ca),[6–8] we have reported the existence of ferromagnetic and/or canted antiferromagnetic characteristics. Recently, an elaborate study of the electron doping effect on the magnetic properties in $Sr_{2-x}La_xMnWO_6$ ($0 \leq x \leq 1$) showed a contribution of weak ferromagnetism or canted antiferromagnetism, increasing in importance with increasing x.[9]

In this paper, we discuss the effect of electron doping on structural and magnetic properties in $Sr_{2-x}La_xMnWO_6$ (x=0, 0.25, and 0.5). Our compositions and results differ from the results of Lin *et al.*[9] Electron doping is achieved by appropriate substitution of the divalent alkaline earth by trivalent lanthanide. The compounds have been synthesized in single-phase form, and x-ray diffraction, neutron diffraction, and magnetization studies have been undertaken. In the low temperature neutron diffraction patterns, at temperatures below 10 K, the intensity of the antiferromagnetic reflections decreased with La^{3+} doping and disappeared at 25% La content.

SYNTHESIS AND CHARACTERIZATION

Samples of $Sr_{2-x}La_xMnWO_6$ (x=0.0, 0.25, and 0.5) were prepared from stoichiometric amounts of high purity $SrCO_3$, La_2O_3, MnO, and WO_3. The starting materials were carefully mixed in an agate mortar in the presence of ethanol and the mixed powder was placed in an alumina crucible and calcined at 1223 K for 15 h. The sample was pressed into a pellet and reacted at 1373 K for 48 h, 1473 K for 48 h, 1523 K for 48 h, and 1723 K for 12 h in an Ar+5% H_2 environment. The sample was reground in each step, and grinding and pelleting cycles were carried out to ensure the homogeneity of the sample. The samples were heated and cooled at a rate of 4°/min under the same atmosphere. The sample corresponding to the parent compound, Sr_2MnWO_6 (x=0), is the same as used in our previous work.[7]

X-ray diffraction patterns were obtained from Guinier film data ($CuK\alpha1 = 1.540\,598$ Å). These data were used to index the pattern. Indexing and refinement of the lattice parameters were made with the programs TREOR90[10] and CHECKCELL.[11] Neutron powder diffraction data were collected at the 50 MW R2 research reactor at Studsvik, Sweden. The double monochromator system consisting of two parallel copper crystals in (220) orientation was aligned to give a wavelength of 1.470(1) Å. The neutron flux at the sample position was approximately 10^6 neutrons $cm^{-2} s^{-1}$. A vanadium was used as the sample holder. The step scan covered the 2θ range of 4°–139.92° with step size of 0.08°. Neutron diffraction data below 5 K were collected at ILL, France, using the D1A diffractometer ($\lambda = 1.91$ Å).

Neutron powder diffraction (NPD) data sets were refined by the Rietveld method using the FULLPROF software.[12] A magnetic phase was included in the refinement as a second phase for which only the Mn cations were defined. Diffraction peak shapes were considered as pseudo-Voigt. Background intensities were described by a Chebyshev polynomial with six coefficients. Peak asymmetry corrections were made during refinements.

ac and dc magnetic measurements were performed in a Quantum Design MPMS-XL superconducting quantum interference device (SQUID) magnetometer. Magnetization versus temperature (T) was studied between 5 and 200 K, following two different protocols: zero field cooled (ZFC) and field cooled (FC). The ZFC magnetization was obtained by cooling the sample to 5 K in zero field, turning on a weak magnetic field ($H = 20$, 500, or 2000 Oe), and measuring the magnetization as the sample warmed up to 200 K. The FC magnetization was subsequently obtained by measuring the magnetization, in the same applied field, as the sample cooled to 5 K. Magnetization versus field measurements were performed at 10 K between 10 and −10 kOe. Frequency dependent ac magnetization versus temperature was studied between 5 and 80 K at four different frequencies, 0.17, 1.7, 17, and 170 Hz.

RESULTS AND DISCUSSIONS

The NPD data were collected at 295 (RT), 10, and 5 K. Room temperature NPD patterns of samples $x = 0.25$ and 0.5 can be well refined in the monoclinic symmetry using the space group $P2_1/n$. In our previous studies, we have shown that the undoped sample crystallizes in the $P4_2/n$ space group.[7] The change of space group from tetragonal $P4_2/n$ (for $x = 0$) to $P2_1/n$ is attributed to the clear matching of the splitting and overlapping reflections. The ionic radius of La^{3+} is smaller than the ionic radius of Sr^{2+}.[13] Substitution of Sr^{2+} by La^{3+} can be well described within the $P2_1/n$ space group. In Glazer's notation, the effect of cation ordering and octahedral tilting is described by $(a^+b^-b^-)$.[14] Figures 1(a) and 1(b) show the observed, calculated, and difference curves after Rietveld refinement of the neutron diffraction data at 295 and 5 K for $Sr_{1.75}La_{0.25}MnWO_6$. The refinements resulted in acceptable R factors and reasonable cell and atomic parameters using the monoclinic $P2_1/n$ space group. Structure parameters, atomic positions, and R factors obtained from the analysis at 295, 10, and 5 K are summarized in Table I. The results show a considerable cell expansion upon La doping. The expansion of the unit cell volume upon doping with a smaller volume cation is opposite to what one expects according to Vegard's law. Therefore, the cell expansion is not motivated by the steric effects associated with the ionic sizes but it reflects electronic effects.

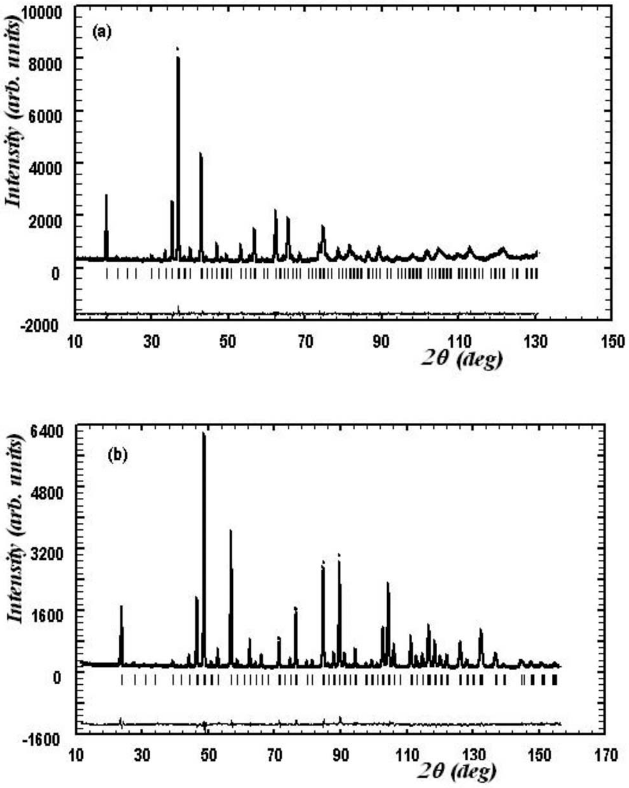

FIG. 1. [(a) and (b)] Observed (circles) and calculated (continuous line) NPD intensity profiles for $Sr_{1.75}La_{0.25}MnWO_6$ at 295 and 5 K. The short vertical lines indicate the angular position of the allowed Bragg reflections. At the bottom in each figure, the difference plot, $I_{obs} - I_{calc.}$, is shown.

The electron doping leads to an expansion of the mean radius of the atomic species at (B, B') sites in the $(A_{2-x}A'_x)BB'O_6$ double-perovskite network. Simultaneously, the reduction of the size of the (A, A') site leads to a reduction of the Goldschmidt tolerance factor t and justifies the reduction of symmetry upon doping. From the Rietveld refinement, we show that there is no mixing of Mn and W species in the (B, B') sites. The $2d$ and $2b$ sites are fully occupied by Mn and W atoms, respectively. The unit cell parameters are related to that of ideal cubic perovskite as $a \approx \sqrt{2}a_p$, $b \approx \sqrt{2}a_p$ and $c \approx 2a_p$ ($a_p \approx 3.89$ Å). Figure 2 shows a schematic polyhedral representation of the double-perovskite structure of $Sr_{1.75}La_{0.25}MnWO_6$ in the space group $P2_1/n$. The monoclinic distortion is very small, with a β angle very close to 90°; this effect has been widely observed in many 1:1 ordered perovskites with a strong pseudo-orthorhombic character. The crystal structures are considerably distorted due to the small size of (A, A') cations, which force the $(Mn,W)O_6$ octahedra to tilt in order to optimize the (Sr/La)–O bond distances. The MnO_6 and WO_6 octahedra are fully ordered and alternate along the three directions in the crystal structure in such a way that each MnO_6 octahedron is linked to six WO_6 octahedra and vice versa (see Fig. 2). We have a so-called NaCl-type ordered double perovskite. The driving force for the B' and B'' orderings is the size and charge difference between both kinds of cations. Figure 3 shows the Rietveld refinement of $Sr_{1.5}La_{0.5}MnWO_6$ at 295 and 10 K.

TABLE I. Main crystallographic and magnetic information for $Sr_{2-x}La_xMnWO_6$ (x=0.25 and 0.5) (e.g., $P2_1/n$, Z=2) from NPD data at different temperatures.

Parameter	$Sr_{1.75}La_{0.25}MnWO_6$			$Sr_{1.5}La_{0.5}MnWO_6$		
Temperature (K)	295	10	5	295	10	5
a (Å)	5.6763(9)	5.6679(7)	5.6599(1)	5.6792(9)	5.6665(8)	5.6605(1)
b (Å)	5.6789(9)	5.6751(7)	5.6677(1)	5.6836(8)	5.6791(8)	5.6734(1)
c (Å)	8.022(1)	8.0062(8)	7.9959(1)	8.0256(1)	8.0105(9)	8.0018(2)
β (deg)	89.94(2)	89.92(2)	89.945(2)	89.97(3)	89.97(3)	89.97(4)
V (Å^3)	258.58(7)	257.53(5)	256.495(6)	259.06(7)	257.78(6)	256.97(1)
Sr/La in $4e(x\ y\ z)$						
x	−0.005(1)	−0.0063(9)	−0.0035(6)	−0.006(1)	−0.0056(1)	−0.005(1)
y	−0.0221(6)	−0.0276(5)	−0.0262(3)	−0.0217(7)	−0.0272(7)	−0.0243(5)
z	0.749(3)	0.749(2)	0.7492(9)	0.751(4)	0.752(2)	0.751(1)
B (Å^2)	0.62(5)	0.44(8)	0.56(5)	0.62(5)	0.35(8)	0.47(6)
Mn in $2d(0\ \frac{1}{2}\ 0)$						
B (Å^2)	0.20(3)	0.24(4)	0.25(4)	0.20(3)	0.45(2)	0.35(2)
W in $2b(\frac{1}{2}\ 0\ 0)$						
B (Å^2)	0.20(7)	0.26(1)	0.26(5)	0.21(2)	0.42(5)	0.25(4)
O1 in $4e(x\ y\ z)$						
x	0.302(2)	0.299(2)	0.2962(8)	0.298(3)	0.299(2)	0.293(1)
y	0.274(2)	0.272(2)	0.2686(8)	0.272(2)	0.270(1)	0.269(1)
z	0.029(2)	0.034(1)	0.0346(7)	0.033(2)	0.034(1)	0.034(1)
B (Å^2)	0.81(8)	0.57(5)	0.56(5)	0.81(8)	0.79(9)	0.78(8)
O2 in $4e(x\ y\ z)$						
x	0.237(2)	0.230(1)	0.2303(9)	0.238(2)	0.235(2)	0.232(1)
y	0.794(2)	0.795(2)	0.7978(7)	0.793(2)	0.796(2)	0.794(1)
z	0.032(2)	0.029(1)	0.0335(7)	0.026(2)	0.036(1)	0.037(1)
B (Å^2)	0.61(1)	0.59(2)	0.55(4)	0.61(1)	0.30(4)	0.81(4)
O3 in $4e(x\ y\ z)$						
x	0.062(2)	0.067(1)	0.0639(6)	0.064(2)	0.069(1)	0.0667(9)
y	0.510(1)	0.5124(8)	0.5117(4)	0.511(1)	0.5127(9)	0.5122(7)
z	0.736(1)	0.7351(9)	0.7377(5)	0.736(2)	0.737(1)	0.7359(9)
B (Å^2)	0.78(8)	0.48(2)	0.54(4)	0.78(8)	0.49(2)	0.49(4)
Reliability factors						
R_p(%)	4.21	4.20	4.78	4.48	4.39	6.80
R_{wp}(%)	5.42	5.40	6.37	5.75	5.70	8.96
R_B(%)	3.09	2.61	5.05	3.69	3.10	7.26
χ^2	1.25	1.25	4.00	1.54	1.54	4.25

Since the sixfold-coordinated ionic radii for Mn^{2+} and W^{6+} ions are 0.97 and 0.74 Å, respectively,[13] there will be a tendency for Mn^{2+} ions to occupy larger octahedral sites than W^{6+} ions. The MnO_6 octahedra are significantly larger than the WO_6 octahedra (see Fig. 2). Due to the $P2_1/n$ symmetry, there is flexibility in the volumes of the individual BO_6 octahedra, thereby permitting a variety of different cation ordering patterns over the B sites. The average B–O bond lengths at 295 K do not show any significant change with electron doping; i.e., for x=0.25, ⟨Mn-O⟩=2.153(5) Å and ⟨W-O⟩=1.927(5) Å and for x=0.5, ⟨Mn-O⟩=2.155(5) Å and ⟨W-O⟩=1.930(5) Å. The main bond lengths, bond valence sums, and octahedral distortions are listed in Table II. At 5 K, the unit cell volume and bond lengths are smaller than at 295 K due to the reduced thermal vibration of the atoms. Calculation of bond valence sums (BVSs) from the structural parameters, using Brown's bond valence model,[15] indicated that Mn and W cations are in mixed-valence states. The calculated valence state of Mn is larger than its initial value (Mn^{2+}) and seems to be a mixture of Mn^{2+} and Mn^{3+}. How-

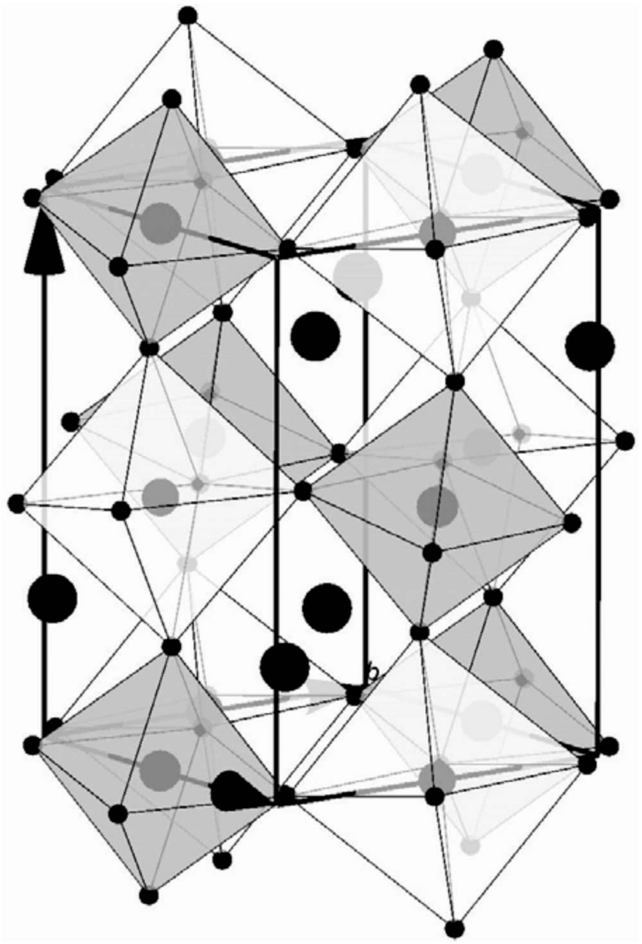

FIG. 2. The three-dimensional crystal structure of the monoclinic perovskite $Sr_{1.5}La_{0.5}MnWO_6$. Sr/La atoms are shown as large black spheres; oxygens are shown as small black spheres at the corner of octahedra. Mn and W are located inside the white and gray octahedra, respectively.

ever, the calculated valence state of W is lower than that of W^{6+}, therefore indicating a mixture of W^{6+} and W^{5+}. Considering the 5 K NPD refinement for accuracy, we have seen that when the average Mn–O bond length decreases, the average W–O bond length instead increases. Since the BVS calculation depends on the average bond distances, when the valence state of W^{6+} decreases, the valence state of Mn^{2+} increases (see Table II). Lin *et al.*[9] have calculated the valence state of similar materials by x-ray absorption spectroscopy (XAS) and showed that the valence state of Mn is +2 and W is mixture of +6 and +5. Since XAS in comparison to NPD is a more accurate method to determine the valence states, we believe that the valence states of Mn and W predominantly are Mn^{2+} and $W^{6+/5+}$, respectively. A strong tilting of the BO_6 octahedra compared with the ideal cubic structure is observed. The MnO_6 octahedra are elongated along the c axis, while the WO_6 octahedra are compressed along the same axis.

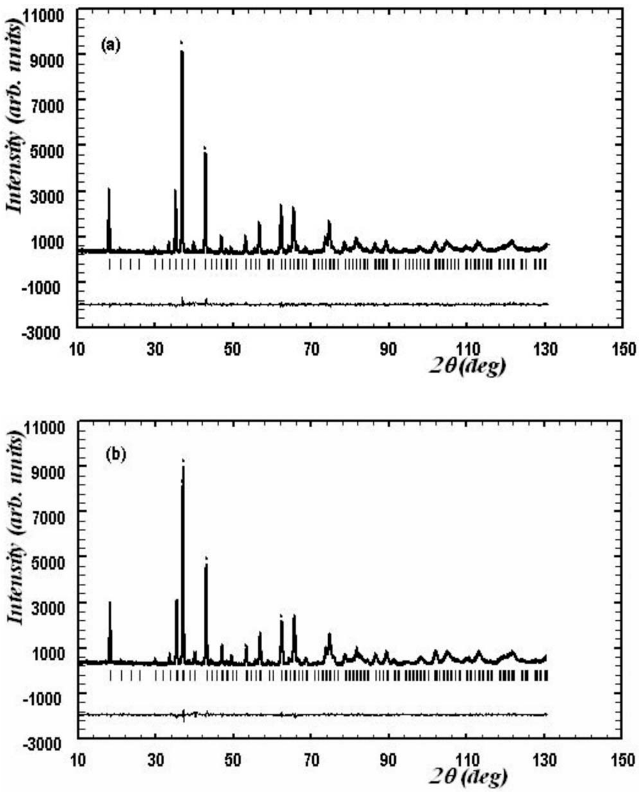

FIG. 3. [(a) and (b)] Observed (dots), calculated (lines), and difference (bottom) plots of NPD Rietveld profiles for $Sr_{1.5}La_{0.5}MnWO_6$ at 295 and 10 K. The short vertical lines indicate the angular position of the allowed Bragg reflections. At the bottom in each figure, the difference plot, $I_{obs}-I_{calc.}$, is shown.

The temperature dependence of the dc susceptibility (χ) for the electron doped samples displays a sharp cusp in the FC curve at T_u, T_u=9.9 and 15.9 K for x=0.25 and 0.5, respectively, and a distinct divergence between the ZFC and the FC curves at temperatures below the cusp temperature (cf. Fig. 4). Moreover, the suppression of the dc susceptibility at $T<T_u$ with increasing applied field as well as the slight decrease of the temperature where the FC and ZFC curves diverge are other characteristic features of these samples. These sample characteristics give a clear indication of a magnetically disordered spin-glass state. Note also the increasing susceptibility with increasing La content, which will be commented on further in Conclusions. The corresponding susceptibility curves for the parent compound, x=0, are included in Fig. 4 for comparison. As discussed in Ref. 7, the parent compound exhibits a transition from a paramagnetic to a short-range canted antiferromagnetic state, consisting of finite-size antiferromagnetic domains, at 50 K, and on further lowering of the temperature, a transition to a long-range antiferromagnetic state at T_N=13 K. The field dependence of the susceptibility of this sample is fundamentally different from the corresponding field dependence observed for the electron doped samples. The sharp susceptibility peak observed at T_N is unaffected by the field strength, while the divergence between the ZFC and FC curves decreases with increasing field and is barely visible for H=2 kOe. All investigated compounds (x=0, 0.25, and 0.5) exhibit a typical Curie-Weiss behavior at high temperatures and fitting a Curie-Weiss law, $\chi=C/(T-\theta)$ to the χ versus T—data in the temperature region of 60–200 K yielded the results given in

TABLE II. Main bond distances (Å) ($d \leqslant 3.5$ Å), octahedral distortion, and bond valence sums for monoclinic $Sr_{2-x}La_xMnWO_6$ ($x=0.25$ and 0.5) determined from NPD data at 295 and 5 K.

	$Sr_{1.75}La_{0.25}MnWO_6$		$Sr_{1.5}La_{0.5}MnWO_6$	
		MnO_6 octahedra		
	295 K	5 K	295 K	5 K
Mn-O1 (Å) (×2)	2.15(1)	2.146(5)	2.15(1)	2.140(6)
Mn-O2 (Å) (×2)	2.16(1)	2.150(5)	2.17(1)	2.153(6)
Mn-O3 (Å) (×2)	2.14(1)	2.129(5)	2.15(1)	2.138(6)
⟨Mn-O⟩(Å)	2.153(5)	2.142(2)	2.155(5)	2.144(3)
Distortion (Δ)	0.074×10^{-4}	0.177×10^{-4}	0.106×10^{-4}	0.104×10^{-4}
Bond valence sums	2.28(3)	2.35(1)	2.31 (3)	2.32(2)
		WO_6 octahedra		
W-O1 (Å) (×2)	1.94(1)	1.930(5)	1.94(1)	1.936(6)
W-O2 (Å) (×2)	1.91(1)	1.928(5)	1.92(1)	1.930(7)
W-O3 (Å) (×2)	1.93(1)	1.936(5)	1.93(1)	1.937(9)
⟨W-O⟩(Å)	1.927(5)	1.931(2)	1.930(5)	1.935(3)
Distortion (Δ)	0.174×10^{-4}	0.035×10^{-4}	0.27×10^{-4}	0.025×10^{-4}
Bond valence sums	5.91(7)	5.85(3)	5.94(8)	5.74(5)
		Sr/LaO_{12} polyhedra		
Sr/La-O1(Å)	3.30(2)	3.295(8)	3.30(3)	3.28(1)
Sr/La-O1(Å)	2.77(3)	2.809(9)	2.82(3)	2.87(1)
Sr/La-O1(Å)	2.83(2)	2.757(7)	2.79(2)	2.72(1)
Sr/La-O1(Å)	2.51(2)	2.527(8)	2.51(3)	2.52(1)
Sr/La-O2(Å)	2.85(3)	2.810(9)	2.88(3)	2.87(1)
Sr/La-O2(Å)	3.26(2)	3.301(8)	3.29(3)	3.31(1)
Sr/La-O2(Å)	2.54(2)	2.513(8)	2.52(3)	2.49(1)
Sr/La-O2(Å)	2.756(2)	2.764(7)	2.73(2)	2.73(1)
Sr/La-O3(Å)	2.685(8)	2.648(3)	2.687(8)	2.674(5)
Sr/La-O3(Å)	3.049(7)	3.074(3)	3.057(8)	3.064(5)
Sr/La-O3(Å)	3.17(1)	3.181(5)	3.18(1)	3.182(8)
Sr/La-O3(Å)	2.52(1)	2.499(5)	2.52(1)	2.496(8)

Table III, where W is assumed to give no contribution to the magnetic moment.[9] The extracted effective moments (μ_{eff}) are in good agreement with the calculated value for the Mn^{2+} moments ($S=5/2$), $5.92\mu_B$, and the results indicate a slight decrease in magnetic moment with increasing electron doping.

The field dependent magnetization at 10 K is shown for all three samples in Fig. 5. A clear hysteresis loop is observed for the $x=0.5$ sample, while for the $x=0.25$ sample, the hysteretic behavior is less pronounced, and $x=0$ shows a predominantly linear field dependence. The increase of the field induced magnetization with increasing electron doping suggests that one important result of this doping is that it creates ferromagnetic couplings in the sample.

Results from ac susceptibility versus temperature measurements are shown in Figs. 6–8. The observed frequency dependence for the in-phase component (χ') and out-of-phase (χ'') components of the ac susceptibility, for samples with $x=0.25$ and $x=0.5$, supports the earlier assumption of a low temperature spin-glass state. Moreover, the magnitude of χ'' for both $x=0.25$ and $x=0.5$ is 2%–3% of the value of χ', which is another characteristic feature of a spin-glass material. From dynamic scaling analysis, assuming the critical slowing down of the spin dynamics according to $\tau=\tau_0\varepsilon^{-z\nu}$, where $\varepsilon=(T-T_g)/T_g$, the values of the spin-glass transition temperature T_g, dynamic critical exponent $z\nu$, and microscopic relaxation time τ_0 can be extracted. Pairs of relaxation times and temperatures are obtained from the cusp temperatures T_f of χ' and the corresponding relaxation times are defined as $\tau(T_f)=1/2\pi f$. The results of the critical scaling analyses are as follows: $T_g=9.9$ K, $z\nu=13.2$, and $\tau_0=2.9\times10^{-13}$ s and $T_g=16.5$ K, $z\nu=11.0$, and $\tau_0=4.3\times10^{-13}$ s for $x=0.25$ and $x=0.5$, respectively, all values being well within the range of values reported for archetypal 3*d* spin-glass materials.[16] As for the parent compound Sr_2MnWO_6 ($x=0$), it is not possible from the ac susceptibility measurements to resolve a frequency dependence in χ' and χ'' within the sensitivity of the experiment zero[17] (cf. Fig. 6). This clearly demonstrates that the splitting between the ZFC/FC curves

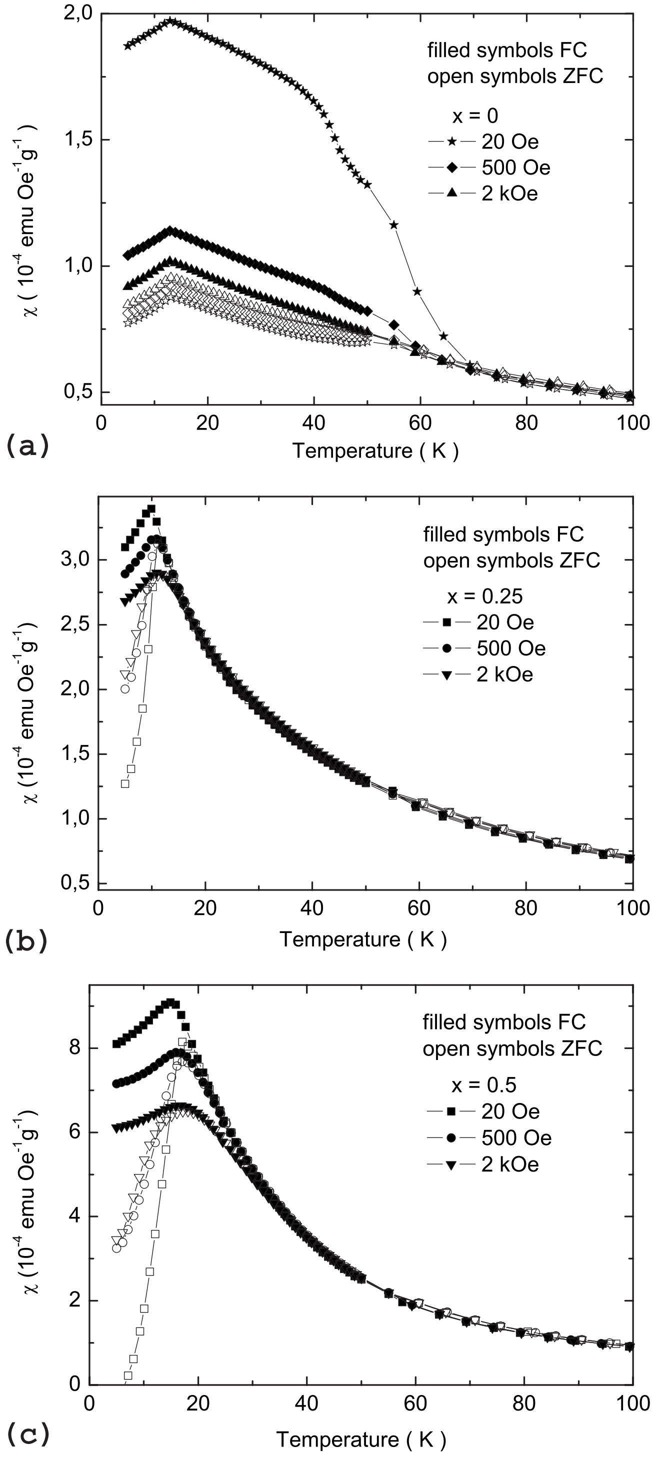

FIG. 4. [(a)–(c)] χ_{ZFC} and χ_{FC} versus temperature for $Sr_{2-x}La_xMnWO_6$, $x=0$ in (a), $x=0.25$ in (b), and $x=0.5$ in (c), measured with the applied fields $H=20$, 500, and 2000 Oe.

for the $x=0$ sample, seen in Fig. 4(a), does not originate from a spin-glass transition.

TABLE III. For different amounts of La ($x=0$, 0.25, and 0.5), the Weiss temperature (θ), Curie constant (C), and effective moment (μ_{eff}) have been extracted from a Curie-Weiss fit of the high temperature region.

x	θ (K)	C (K)	μ_{eff} (μ_B/Mn)
0	−78.3	0.754	6.10
0.25	−4.78	0.625	5.57
0.5	24.5	0.576	5.35

The neutron data at $T=5$ K for the $x=0.25$ sample show a small and broad diffraction peak of magnetic origin that indicates the presence of antiferromagnetic (AF) spin-spin correlations, as shown in Fig. 9. Even though the material has regions of antiferromagnetically ordered magnetic spins, it is clear from the dc and ac susceptibility data that these short-range correlated AF regions coexist with a low temperature spin-glass state. In case of the $x=0.5$ sample, there are no indications of AF spin-spin correlations from the neutron data. The results both from NPD and SQUID measurements clearly suggest that substitution of Sr^{2+} with La^{3+} destroys the AF state seen in pure Sr_2MnWO_6.[7] Electron doping instead yields a disordered and frustrated magnetic state at low temperatures. The low temperature spin-glass state is expected to result from incorporation of randomly distributed ferromagnetic (FM) interactions, the amount of which increases with increasing electron doping (i.e., La concentration). This would explain the change in sign of θ, the increase in magnitude of the field induced magnetization (cf. Fig. 4), as well as the more pronounced hysteretic behavior (cf. Fig. 5) for $x=0.5$ compared to $x=0.25$.

CONCLUSIONS

The B-site ordered double-perovskite-type oxides, $Sr_{2-x}La_xMnWO_6$ ($x=0.25$ and 0.5), crystallize with monoclinic structure. Rietveld analysis of NPD data shows that these compounds are of B-site ordered double-perovskite type and crystallize in the space group $P2_1/n$. A mixture between nearest-neighbor and next-nearest-neighbor superexchange interactions is the probable cause for the magnetic spin-glass behavior seen for both samples. To understand the

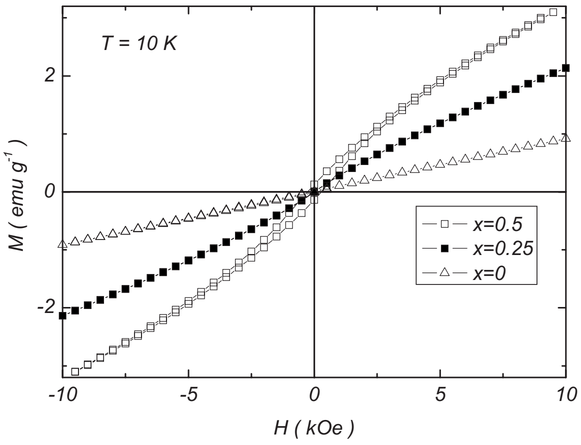

FIG. 5. Magnetization (M) versus applied field (H) at $T=10$ K for $Sr_{2-x}La_xMnWO_6$; square, circle, and triangular symbols correspond to $x=0.5$, 0.25, and 0, respectively.

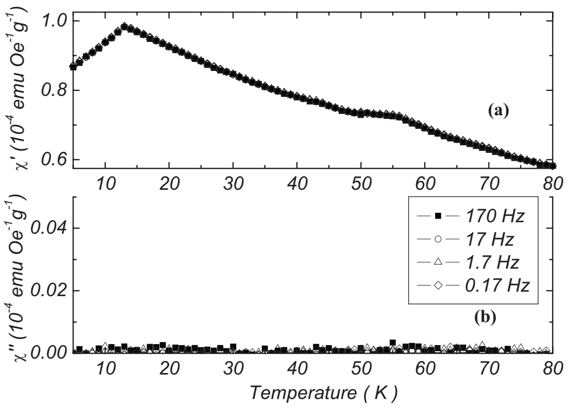

FIG. 6. [(a) and (b)] Frequency dependent ac susceptibility versus temperature for the ac field frequencies of 0.17, 1.7, 17, and 170 Hz for $x=0$.

ferromagnetic Mn-Mn exchange interaction, the electron configuration of W must be understood and hence the occurrences of a mixed W^{6+}/W^{5+} valence. Without electron doping, only W^{6+} exists that has filled electron shells with $5d^0$, and hence there is no nearest-neighbor exchange interaction between Mn^{2+} and W^{6+} moments. Thus, the next-nearest-neighbor superexchange interaction, Mn-O-W-O-Mn, will dominate producing the AF order[18] seen in NPD measurements at low temperature for $x=0$.[7] Through electron doping, substituting Sr^{2+} for La^{3+}, an admixture of W^{5+} (d^1) and W^{6+} (d^0) is formed,[19] thus creating a mixed-valence state for the W ions. W^{5+} acts as a Pauli paramagnetic ion whose exchange polarization supports a FM Mn-Mn interaction[9] and a mixture of both AF and FM interactions is thus created. The FM Mn-Mn interactions can be understood as follows: The first Mn^{2+} moment will experience an AF superexchange interaction with W^{5+} through an O $2p$ orbital, and the next Mn moment will experience a similar AF exchange with the same W ion, resulting in an indirect exchange between the two Mn^{2+} moments (Mn-O-W-O-Mn) that will be FM. This explains the difference in magnitude seen in the field induced magnetization (cf. Fig. 4) between the $x=0.25$ and $x=0.5$ samples, since an increase in electron doping (increase of x) will result in an increasing number of ferromagnetic interactions. The La^{3+} substitution of Sr^{2+} will occur randomly in the material leading to randomly distributed FM exchange interactions between the Mn moments, thus creating the prerequisite conditions, i.e., a disordered mix of AF and FM interactions, to form a low temperature spin-glass phase. Hence, a magnetically disordered and frustrated spin system is created upon electron doping in the $Sr_{2-x}La_xMnWO_6$ system.

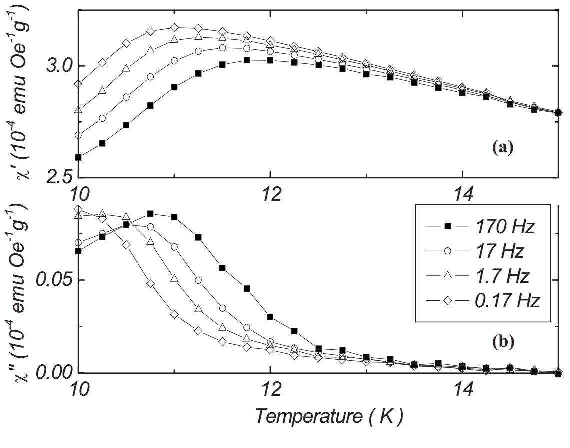

FIG. 7. [(a) and (b)] Frequency dependent ac susceptibility versus temperature for the ac field frequencies 0.17, 1.7, 17, and 170 Hz for $x=0.25$.

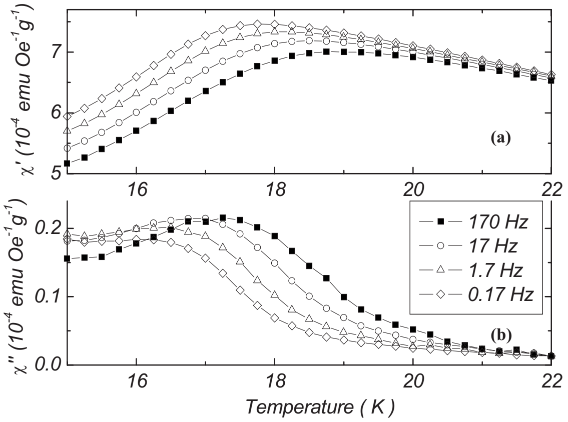

FIG. 8. [(a) and (b)] Frequency dependent ac susceptibility versus temperature for the ac field frequencies 0.17, 1.7, 17, and 170 Hz for $x=0.5$.

ACKNOWLEDGMENTS

The authors are grateful to the Swedish Foundation of Strategic Research (SSF), the Swedish Research Council (VR), and the Knut and Alice Wallenberg Foundation (KAW) for financial support. A.K. Azad is grateful for all types of support from Bangladesh Atomic Energy Commission and A. Khan is grateful for the financial support from HEC, Pakistan.

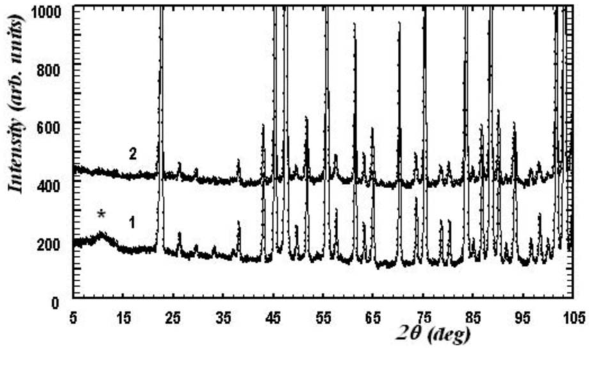

FIG. 9. Observed NPD patterns for $Sr_{2-x}La_xMnWO_6$ ($x=0.25$ and 0.5) at 5 K to locate the magnetic reflections. Magnetic reflection is indicated by *.

[1] K.-I. Kobayashi, T. Kimura, H. Sawada, K. Terakura, and Y. Tokura, Nature (London) **395**, 677 (1998).

[2] O. Chmaissem, R. Kruk, B. Dabrowski, D. E. Brown, X. Xiong, S. Kolesnik, J. D. Jorgensen, and C. W. Kimball, Phys. Rev. B **62**, 14197 (2000).

[3] B. Garcia-Landa, C. Ritter, M. R. Ibarra, J. Blasco, P. A. Algarabel, R. Mahendiran, and J. Garcia, Solid State Commun. **110**, 435 (1999).

[4] C. Ritter, M. R. Ibarra, L. Morellon, J. Blasco, J. Garcia, and J. M. De Teresa, J. Phys.: Condens. Matter **12**, 8295 (2000).

[5] C. Ritter, J. Blasco, and J.-M. De Teresa, D. Serrate, L. Morellon, J. Garcia, and M. R. Ibarra, Solid State Sci. **6**, 419 (2004).

[6] A. K. Azad, S.-G. Eriksson, S. A. Ivanov, H. Rundlöf, J. Eriksen, R. Mathieu, and P. Svedlindh, Ferroelectrics **269**, 105 (2002).

[7] A. K. Azad, S. A. Ivanov, S.-G. Eriksson, H. Rundlöf, J. Eriksen, R. Mathieu, and P. Svedlindh, J. Magn. Magn. Mater. **237**, 124 (2001).

[8] A. K. Azad and S.-G. Eriksson, Solid State Commun. **126**, 503 (2003).

[9] Q. Lin, M. Greenblatt, and M. Croft, J. Solid State Chem. **178**, 1356 (2005).

[10] P.-E. Werner, L. Eriksson, and M. Westdahl, J. Appl. Crystallogr. **18**, 367 (1985).

[11] J. Laugier and B. Bochu, Checkcell: Graphical Powder Indexing, Cell and Space Group Assignment Software (http://www.inpg.fr/LMGP).

[12] J. Rodrigues-Carvajal, Physica B **192**, 55 (1993).

[13] R. D. Shannon, Acta Crystallogr., Sect. A: Cryst. Phys., Diffr., Theor. Gen. Crystallogr. **32**, 751 (1976).

[14] A. M. Glazer, Acta Crystallogr., Sect. B: Struct. Crystallogr. Cryst. Chem. **28**, 3384 (1972).

[15] I. D. Brown, in *Structure and Bonding in Crystals*, edited by M. O'Keefe and A. Navrotsky (Academic, New York, 1981) Vol. 2, pp. 1–30.

[16] P. Nordblad and P. Svedlindh, in *Spin Glasses and Random Fields*, edited by A. P. Young (World Scientific, Singapore, 1997), pp. 251–275.

[17] Sensitivity 2×10^{-8} emu, MPMS ac susceptibility measurement option (http://www.qdusa.com/products/mpms.html).

[18] J. B. Goodenough, *Magnetism and The Chemical Bond* (Interscience, New York, 1963).

[19] E. N. Caspi, J. D. Jorgensen, M. V. Lobanov, and M. Greenblatt, Phys. Rev. B **67**, 134431 (2003).